C-3

NATIONAL ADVISORY COMMITTEE FOR AERONAUTICS

TECHNICAL MEMORANDUM

No. 1150

COMPRESSION SHOCKS OF DETACHED FLOW

By Eggink

Translation

"Uber Verdichtungsstösse bei abgelöster Strömung"

Deutsche Luftfahrtforschung, Forschungsbericht Nr. 1850

Washington
June 1947

NACA TM No. 1150

COMPRESSION SHOCKS OF DETACHED FLOW

By Eggink

June 1947

Every effort is made by the NACA to insure that its published translations are accurate reproductions of the original work of the authors. Papers are selected for translation on the basis of interest and probable usefulness and, although an examination is made for technical soundness, the Committee cannot assume responsibility for the accuracy of the detailed results presented by the author in the original paper. The Committee will of course call attention to any errors observed at the time of publication or subsequent thereto.

Analysis of NACA Technical Memorandum No. 1150 has disclosed that the principal result of the original paper is in error. The compatibility of the three branches of a λ-shock (Y-shock, branch-shock, fork-shock) in a supersonic flow is granted at crossing points of two supersonic arcs corresponding to two opposite families of characteristics and one common subsonic arc ending at the sonic line. The further continuation is sometimes rather the characteristic of the same family than the supersonic arc of the shock polar itself corresponding to the opposite family. Such cases with characteristics are not considered by Eggink. Therefore, his classification of λ-shocks and the sensational result that λ-shocks cannot exist below Mach number 1.245 is without any value. Obviously λ-shocks are possible at all supersonic velocities and their appearance is without any special physical significance.

NATIONAL ADVISORY COMMITTEE FOR AERONAUTICS

TECHNICAL MEMORANDUM NO. 1150

COMPRESSION SHOCKS OF DETACHED FLOW*

By Eggink

SUMMARY

It is known that compression shocks which lead from supersonic to subsonic velocity cause the flow to separate on impact on a rigid wall. Such shocks appear at bodies with circular symmetry or wing profiles on locally exceeding sonic velocity, and in Laval nozzles with too high a back pressure. The form of the compression shocks observed therein is investigated.

I. INTRODUCTION

The present investigation of the forms of shock proceeded from schlieren observations of wing profiles and an investigation of the forms of shock in Laval nozzles with too high a back-pressure. Schlieren photographs of the shock forms in Laval nozzles have been published already in FB 1756.

In observing shock it is necessary to be sure to have a suitable adjustment of the schlieren optical system. Good definition of the shock form can be obtained with the schlieren edge perpendicular to the flow, and bright shock lines against a dark field. Small tunnel breadth yields sharp shock lines, while the shock is no longer perfectly plane and appears streaked. The observation is often disturbed by violent fluttering of the shock. Then the shock appears to the eye as a broad streaked band and in photographs, as a set of shocklines. (Compare fig. 3.)

---

*"Über Verdichtungsstösse bei abgelöster Strömung," Zentrale für wissenschaftliches Berichtswesen der Luftfahrtforschung des Generalluftzeugmeisters (ZWB) Berlin-Adlershof, Forschungsbericht Nr. 1850, Aachen, Aug. 12, 1943.

II. THE ASSORTED SHOCK FORMS

It will be assumed that there is a compression shock in a supersonic flow. If this shock encounters a rigid wall, there are three cases to distinguish. (See figs. 1(a) to 1(c).)

(a) The shock runs perpendicular to the wall; the flow does not separate.

(b) The shock runs oblique to the wall; the flow separates from the wall.

(c) The shock branches into two separated shocks in front of the wall.

In case (b) the flow generally returns to the wall after flowing past the dead space, since the pressure gradient directed against the wall downstream from the bent shock forces the streamlines against the wall. From the observation that the flow behind the shock is along the wall again, it cannot be inferred, therefore, whether case (a) or (b) is present. (Compare fig. 2.)

In contrast to case (b), which is observed shortly after exceeding sonic velocity, the branch of (c) (fig. 3) is first observed at higher Mach numbers. In agreement with this, it follows from the theory of the branching in Section III, that a branching first comes into existence for

$$M^* = \frac{w}{a^*} > 1.191$$

or

$$M = \frac{w}{a} > 1.245$$

The schlieren observations of the branch show, that the principal shock A-D is bent, in general, and the branch shock lines A-B and A-C can be regarded as practically straight. By this the stream boundary B-C is taken as straight and the pressure is assumed constant in the dead space along this boundary. (If the flow is already detached weakly upstream by considerable roughness of the wall, then a fan of shock lines, which come together in the principal shock forms in place of the branch.)

The flow in the vicinity of the branch point is computed in Section III.[1] This gives as a result the shocks coming together at the branch point A and, with that, the shock lines A-B and A-C as functions of the flow and the diversion of the flow in the separation point B or the pressure in the lead space.

III. THEORY OF BRANCHING

1. Statement and Execution of the Solution

The individual compression shocks coming together in the point A are shown in the familiar shock-polar diagram of A. Busemann. The streamline A-E, which passes through the branch point, separates the two flows (3) and (4) (fig. 4) behind the shock.

The pressure P in (3) and (4) must be equal along this boundary, and the directions of the velocities in (3) and (4) be parallel to it. The different increase of entropy from (1) to (4) and (1) to (3) yields a discontinuity in the velocity, temperature, and density across the boundary.

The flow (1) corresponds to the shock pole M_1^* in the polar diagram (fig. 4) on which (2) and (4) lie. (3) lies on the shock pole M_2^* which was defined by means of (2), which is variable.

The conditions required at the separation line:

$$p_3 = p_4$$

$$\delta_2 + \delta_3 = \delta_4 \qquad (1)$$

suffice to ascertain the points (3) and (4) for each M_2^* or δ_2.

In the dimensionless formulas for the compression shock the pressure p is referred to the static pressure of the flow, p_0 $\left(\frac{p}{p_0}\right.$ pressure ratio$\left.\right)$. The crooked shock A-B from (1) to (2)

[1] As can be seen in the Techn. Berichten Bd. 10 (1943). Heft 2, Prof. A. Weise DVL likewise worked with branch shocks and computed the special case of branching with a straight principal shock.

reduces the static pressure to $\hat{p}_o$. On the shock polar M_2^* the pressure is therefore to be referred to $\hat{p}_o$. The abbreviation x is used for the pressure ratio of the flow that characterizes the shock polar, the abbreviation y for the pressure ratio along the shock polar, and indicate with the pressure ratio referred to p_o. According to figure 4:

$$\frac{p_1}{p_o} = x_1 \qquad \frac{p_2}{\hat{p}_o} = x_2'$$

$$\frac{p_2}{p_o} = y_2 \qquad \frac{p_3}{\hat{p}_o} = y_3'$$

$$\frac{p_4}{p_o} = y_4$$

Equation (1) is referred to p_o yields:

$$y_3' \frac{\hat{p}_o}{p_o} = y_4$$

$$\vartheta_2 + \vartheta_3 = \vartheta_4 \qquad (2)$$

The ratio of the static pressures $\frac{\hat{p}_o}{p_o}$ is known to be a function of y_2 and x. The formulas for the compression shocks are assumed as known.[2]

The angle of deflection ϑ of the flow follows as a function of y and x from:

---

[2]For further detail concerning the fundamental equations of the compression shock and the formulas derived therefrom, see: R. Sauer "Theoret. Einführung in die Gasdynamik," Springer 1943. The designations chosen there have been retained here.

$$\vartheta = f(x,y) = \arctan\left(\sqrt{\frac{4k}{k^2-1}x^{\frac{1}{k}} - \frac{k+1}{k-1}x - y}\ \frac{y - x^{\frac{1}{k}}}{\frac{2k}{k-1}x^{\frac{1}{k}} - \frac{k+1}{k-1}x - y}\right) \qquad (3)$$

and the static-pressure ratio $\frac{\hat{p}_o}{p_o}$ as a function of the flow x_1 and y_2 from:[3]

$$\frac{\hat{p}_o}{p_o} = \varphi(x_1,y_2) = \left(\frac{k+1}{k-1}\right)^{\frac{k}{k-1}} \left(\frac{x_1}{y_2}\right)^{\frac{1}{k}} \left(\frac{y_2 + \frac{k-1}{k+1}x_1}{y_2 + \frac{k+1}{k-1}x_1}\right)^{\frac{k}{k-1}} \qquad (4)$$

if equation (3) is set up with the same indices as in equation (2):

$$f(x_1,y_4) = f(x_1,y_2) + f(x_2',y_3')$$

and with the use of equation (4):

$$x_1' = \frac{y_2}{(\hat{p}_o/p_o)} = \frac{y_2}{\varphi(x_1,y_2)}$$

as well as $y_3' = \frac{y_4}{\varphi(x_1,y_2)}$ from equation (2).

---

[3] Eliminating the shock angle σ from equations (129) and (130) on page 65 of "Theoret. Einfuhrung i.d. Gasdynamik," leads to equation (3); correspondingly, equation (4) is obtained from equation (129) page 65 and equation (150) page 77.

$$f(x_1,y_4) = f(x_1,y_2) + f\frac{y_2}{\varphi(x_1,y_2)}, \frac{y_4}{\varphi(x_1,y_2)}$$

it is seen that the unknown y_4 cannot be computed explicitly as a result of the complicated function f.

The solution of equation (2) is obtained graphically. The following construction is suitable to this end (fig. 5). The ϑ distribution of the shock polar M_1^* ($= M_1^*$ – distribution) $\vartheta = f(x_1,y)$ from equation (3) is plotted against the pressure ratio y. The ϑ distribution of the shock polar M_2^* ($= M_2^*$ – distribution) is plotted against $y\frac{\hat{p}_o}{p_o}$ displaced parallelwise by ϑ_2. The exaggeration of the y-axis by the factor $\frac{\hat{p}_o}{p_o}$ refers the pressure of the shock polar M_2^* to p_o. With that, the starting point x_2', since $x_2'\frac{\hat{p}_o}{p_o} = y_2$ at the point ϑ_2, coincides with y_2 of the M_1^* – distribution. The points of intersection of the two distributions furnish the desired solution, since the conditions of equations (2) are satisfied here with $\vartheta_2 + \vartheta_3 = \vartheta_4$ and $y_3'\frac{\hat{p}_o}{p_o} = y_4$.

In carrying out the construction, the ϑ distributions were computed for $M_1^* = 1.1; 1.2; \ldots 2.2; 2.3$ and for M_2^* at any instant the smaller value was chosen, for example, for $M_1^* = 2.0$, $M_2^* = 1.9; 1.8; \ldots$ For M_1^* there are intervals in which the solution shows various relations. The boundary values for these intervals as well as the "limiting points" mentioned in the following are treated in the next section.

The manner in which the various solutions in the individual intervals are accounted for in terms of relation of intersection points is schematically illustrated in Section 6–8.

If $1.191 \geqq M_1^* > 1$ then the M_2^* – distribution lies in the interior of the M_1^* – distribution (fig. 6). A branching of the shock does not take place in this region, therefore.

The interval $1.842 \geqq M_1^* > 1.191$ provides a point of intersection (fig. 7). At the starting point x_1 the M_2^* – distribution coincides with the M_1^* – distribution. The M_2^* – distribution

displaced from x_1 with respect to the M_1^* – distribution by a differential shows the "limiting point" a. The point of intersection moves out from a with diminishing M_2^* along the M_1^* – distribution up to the limiting point b. On the variable M_2^* – distributions, the intersection point approaches the starting point y_2 of the M_2^* – distribution, in doing so. At the limiting point b, the intersection point coincides with the starting point of the M_2^* – distribution. Here M_2^* reaches a lower limit below which there is no solution, since the M_2^* – distribution lies within the M_1^* – distribution for smaller values of M_2^*.

If $M_1^* > 1.842$, there are two points of intersection, which run out from the limiting points a and c (fig. 8). At the limiting point a, the variation of the one intersection point known from the preceding interval commences, and terminates at the limiting point b. The second intersection point starts out at the limiting point c and coincides at the limiting point d with the starting point of the appropriate M_2^* – distribution and, thereby, terminates the ambiguity. Near a lower limit for M_2^*, below which there is no longer a solution (limiting point b) there is a lower limit at which the ambiguity vanishes (limiting point d).

2. Obtaining the Limiting Values Limiting Points a and c

At the intersection point of the M_1^* – distribution and M_2^* – distribution, displaced by Δx, $\vartheta' = f(x_1 + \Delta x)\,\frac{\hat{p}_o}{p_o}\,y'\,\frac{\hat{p}_o}{p_o}$ the following is valid according to figure 9:

$$\vartheta = \vartheta' + \Delta\vartheta \qquad y'\,\frac{\hat{p}_o}{p_o} = y = y_g$$

or

$$f\left[(x_1 + \Delta x)\,\frac{\hat{p}_o}{p_o}\,y_g\right] - f(x_1, y_g) = -\Delta\vartheta$$

and

$$\lim_{\Delta x \to 0} \frac{\left[f(x_1 + \Delta x)\,\frac{\hat{p}_o}{p_o}\,y_g\right] - f(x_1, y_g)}{\Delta x} = -\lim_{\Delta x \to 0} \frac{\Delta\vartheta}{\Delta x}$$

and right side goes to $\tan \beta_1$ in the transition at the limit, according to figure 9; this is the direction of the M_1^* - distribution at x_1.

It is:

$$\tan \beta_1 = \frac{\partial f(x_1, y)}{\partial y}_{y = x_1}$$

the left side goes over the partial derivative of f with respect to x at $x = x_1$ since $\frac{\hat{p}_o}{p_o} \longrightarrow 1$ for $\Delta x \longrightarrow 0$. It follows that

$$\frac{\partial f(x, y_g)}{\partial x}_{x = x_1} = - \frac{\partial f(x_1, y)}{\partial y}_{y = x_1} \tag{5}$$

The quantity y_g which defines the limiting points a and c is computed from equation (5). Differentiation of equation (3) yields:

$$\tan \beta_1 = \frac{\partial f(x_1, y)}{\partial y}_{y = x_1} = \frac{\sqrt{k - 1}}{2k} \frac{\sqrt{2 - (k + 1) x_1^{\frac{k-1}{k}}}}{x_1^{\frac{k+1}{2k}} \left(1 - k_1^{\frac{k-1}{k}}\right)} \tag{6}$$

and

$$\left(\frac{\partial f(x,y_g)}{\partial x}\right)_{x=x_1} = \frac{1}{2}\sin 2\vartheta \left[\frac{\left(\frac{4}{k^2-1}x_1\right)^{\frac{1}{k}} - \frac{k+1}{k-1}x_1}{2x_1\left(\left(\frac{4k}{k^2-1}x_1\right)^{\frac{1}{k}} - \frac{k+1}{k-1}x_1 - y_g\right)} \right.$$

$$- \frac{\left(\frac{2}{k-1}x_1\right)^{\frac{1}{k}} - \frac{k+1}{k-1}x_1}{x_1\left(\left(\frac{2k}{k-1}x_1\right)^{\frac{1}{k}} - \frac{k+1}{k-1}x_1 - y_g\right)}$$

$$\left. - \frac{\frac{k-1}{k+1}}{2\left(y_g + \frac{k-1}{k+1}x_1\right)} - \frac{1}{y_g - x_1} \right] \qquad (7)$$

in which ϑ is to be taken from equation (3) with $x = x_1$ and $y = y_g$.

The quantity y_g, defining the limiting points a and c can be obtained only by approximation from equations (5), (6), and (7).

Limiting Points b and d

According to figures (7) and (8) the intersection point of the M_1^* - and the M_2^* - distribution falls on the limiting

points b or d at the starting point of the M_2^* - distribution. Here, therefore, both curves have two points in common, that is, they have a common tangent, or the direction of the M_1^* - distribution = tan α_2 at the point y_2 agrees with the direction of the M_2^* - distribution at the starting point = tan β_2.

$$\tan \alpha_2 = \tan \beta_2 \tag{8}$$

The direction at the starting point of the M_2^* - distribution follows from differentiation of equation (3). (Compare equation (6).)

$$\tan \beta_2 = \frac{1}{\hat{p}_o/p_o} \left.\frac{\partial f(x_2', y_2')}{\partial y'}\right|_{y' = x_2}$$

$$\frac{1}{\hat{p}_o/p_o} \frac{\sqrt{k-1}}{2k} \cdot \frac{\sqrt{2 - (k+1)\, x_2'^{\frac{k-1}{k}}}}{x_2'^{\frac{k+1}{2k}} \left(1 - x_2'^{\frac{k-1}{k}}\right)}$$

In the denominator the exaggeration of the y-axis by the factor $\frac{\hat{p}_o}{p_o}$, mentioned above for the M_2^* - distribution, must be taken into consideration. If

$$x_2' = \frac{p_2}{\hat{p}_o} = \frac{p_2}{p_o} \frac{1}{\hat{p}_o/p_o} = y_2 \frac{1}{\hat{p}_o/p_o}$$

and $\frac{\hat{p}_o}{p_o}$ from equation (4) are substituted, it follows after calculation:

$$\tan \beta_2 = \frac{k-1}{2k\sqrt{k-1}} \frac{\sqrt{\left[2k_1 \left(\frac{k-1}{k+1} x_1 + y_2\right)^{\frac{1}{k}} - (k-1)\, y_2 \left(y_2 + \frac{k+1}{k-1} x_1\right)\right]\left(y_2 + \frac{k+1}{k-1} x_1\right)}}{y_2}$$

$$\times \frac{1}{x_1 \left(\frac{k-1}{k+1} x_1 + y_2\right)^{\frac{1}{k}} - \frac{k-1}{k+1} y_2 \left(y_2 + x_1 \frac{k+1}{k-1}\right)} \qquad (9)$$

Differentiation of equation (3) gives the direction of the M_1^*- distribution at the point $y = y_2$ with ϑ from equation (3) as:

$$\tan \alpha_2 = \frac{1}{2} \sin 2\vartheta \left[\frac{1}{\frac{2k}{k-1} x_1 \left(\frac{1}{k}\right)^{\frac{1}{k}} - \frac{k+1}{k-1} x_1 - y_2} + \frac{1}{y_2 - x_1} - \frac{1}{2\left(y_2 + \frac{k-1}{k+1} x_1\right)} \right.$$

$$\left. - \frac{1}{2\left(\frac{4k}{k^2-1} x_1 \left(\frac{1}{k}\right)^{\frac{1}{k}} - \frac{k-1}{k+1} x_1 - y_2\right)} \right] \qquad (10)$$

Here too, the quantity y_2 sought for is obtained only as an approximation from equations (8), (9), and (10).

The Interval Limits

Figures 10 to 12 show the variation of the curves $\tan \alpha_2$ and $\tan \beta_2$ with y_1 for fixed M_1^*, in the various intervals. The intersection points of both curves furnish the y_2 - values of the limiting points b and d.

Both intersection points approach the starting point x_1 of both curves with diminishing M_1^*. First of all, d, coincides with x_1; because of this ambiguity vanishes, since only the limiting point b still exists. The variation in curve of figure 10 goes over to the variation of the curve in figure 11. Then b coincides with x_1 and the variation of the curve corresponds to figure 12. The vanishing of the limiting point b is only possible, however, if the M_2^* - distribution lies within the M_1^* - distribution. Here the lower limit for M_1^* is reached, accordingly, below which there is no solution. The curves $\tan \alpha_2$ and $\tan \beta_2$ agree at the point $y = x_1$ in magnitude and direction, that is:

$$\tan \alpha_2 = \tan \beta_2 \tag{11}$$

$$\frac{\partial \tan \alpha_2}{\partial y} = \frac{\partial \tan \beta_2}{\partial y} \tag{12}$$

The somewhat detailed proof of these relations by equating and differentiating equations (9) and (10) is passed over here.

Since the directions of both curves at the point x_1 agree, the coincidence of the intersection points b and d with x_1 means that the curvature of both curves agree at the point x_1. Therefore, with equation (12) the two second derivatives of both curves are equal.

$$\frac{\partial^2 \tan \alpha_2}{\partial y^2} = \frac{\partial^2 \tan \beta_2}{\partial y^2} \qquad (13)$$

The interval limits sought for follow from equation (13).

Taking the partial derivative of equations (9) and (10) and substituting in equation (13) leads after a detailed calculation, which will not be entered into here, to an algebraic equation of the fourth degree in x_1. By means of the solutions $x_{1a} = 1$ and $x_{1b} = 1$, these reduce to the following equation of the second degree:

$$\left(x_1^{\frac{k-1}{k}}\right)^2 + 2(k - 2)\left(x_1^{\frac{k-1}{k}}\right) - \frac{3k - 5}{k + 1} = 0$$

with the solution:

$$x_1^{\frac{k-1}{k}} = -(k - 2) \pm \sqrt{\frac{k - 1}{k + 1}}$$

or with:

$$x_1^{\frac{k-1}{k}} = 1 - \frac{k - 1}{k + 1} M_1^{*2}$$

solved for M_1^*:

$$M_1^{*2} = (k + 1)\left(1 \pm \sqrt{\frac{k - 1}{k + 1}}\right)$$

This gives: The lower limit for the ambiguity lies at $M_1^* = 1.842$ or $M_1 = 2.568$; the limit, below which there is no solution, lies at $M_1^* = 1.191$ or $M_1 = 1.245$.

3. Plotting the Polar-Shock Diagram

The result of the construction and calculation is displayed in the polar-shock diagram (see appendix).

ϑ_3 is given, with calculated value for y_4, according to figure 5 and the point (3) according to figure 4. The points (3) are computed for the flow M_1^* at any given instant are plotted on the variable-shock polars M_2^*, and joined (fig. 13) by a curve. The curves begin at the shock polar M_1^*, at the limiting point a or c and end on the axis of the diagram at M^* that corresponds to the limiting points b and d. In the shock-polar diagram the point (4) or ϑ_4 (fig. 4), for given point (3) or ϑ_3, is defined from equation (2):

$$\vartheta_4 = \vartheta_2 + \vartheta_3$$

Whether (4) lies on the supersonic or the subsonic side of the shock-polar follows from the variation of additional points. The lower limiting line for M_2^*, below which there is no branching, is the connecting line of the limiting points b (curve b). The lower limiting line for the ambiguity is the connecting of the limiting points d (curve d).

The values of M_2^* for which $\vartheta_4 = 0$, therefore, for which the shock A-D becomes straight, are determined from the intersection point of the curve e marked with little lines with the shock polar M_1^*. If e coincides with the starting point of the shock polar, then the limiting point a must lie on the axis of the diagram, since the limiting point a corresponds to the "solution" at the starting point of the shock-polar and $\vartheta_4 = 0$. This condition used in equation (5), (6), and (7) yields:

$$x_1 = \left(\frac{2}{k+1}\right)^{\frac{2k}{k-1}} \quad \text{or} \quad M_1^* = \sqrt{\frac{k+1}{k-1}\left[1 - \left(\frac{2}{k+1}\right)^2\right]} = 1.353$$

as the intersection point of the curve e with the axis of the diagram. (It is know that the maximum of the pressure for this value is behind a straight shock.)

In figure 14 the branching with straight principal shock is shown for various M_1^*, in figure 15 the branching with fixed $M_1^* = 1.5$ and ϑ_2 variable.

IV. SUMMARY

Schlieren observations show a branching of the compression shock in the vicinity of a fixed wall. The flow in the vicinity of the branching point is computed, and the result displayed in a shock-polar diagram.

A branching of the shock only appears for $M_1^* > 1.191$ ($M_1 > 1.245$). If $M_1^* > 1.842$ ($M_1 > 2.546$), then two solutions exist. If M_1^* lies between 1.191 and 1.353 the principal shock is oblique, the branching deflects the flow direction positively, only for $M_1^* > 1.353$ ($M_1 > 1.484$) the flow direction is deflected both positively and negatively. Here a branching with a straight principal shock becomes possible. The second solution for $M_1^* > 1.842$ yields only a positive deflection of the flow direction.

Translated by Dave Feingold
National Advisory
Committee for Aeronautics

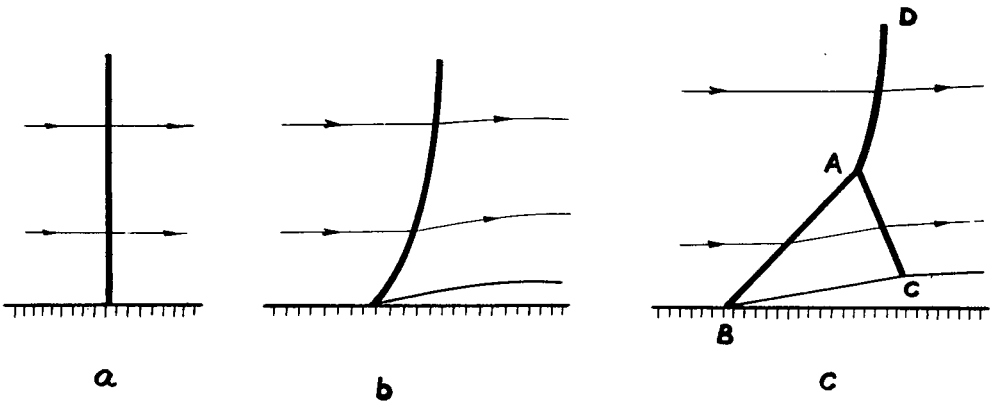

Figure 1. a-c The different shock forms.

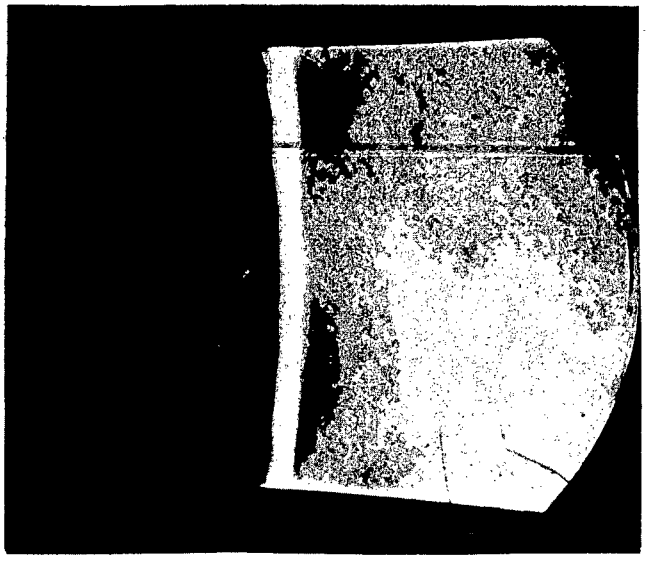

Figure 2. Shock form in a Laval nozzle.

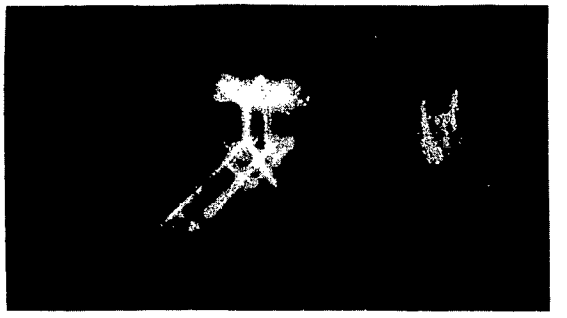

Figure 3b.

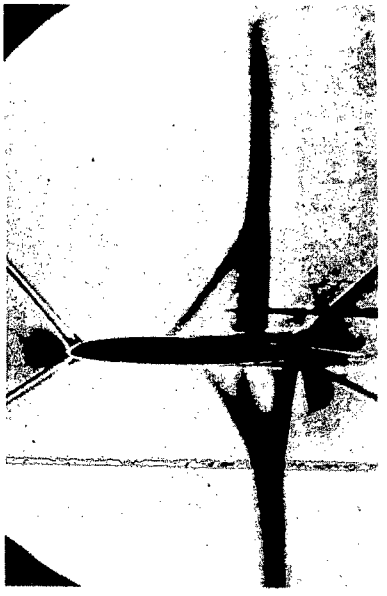

Figure 3a. At a wing profile (taken by Ackered)

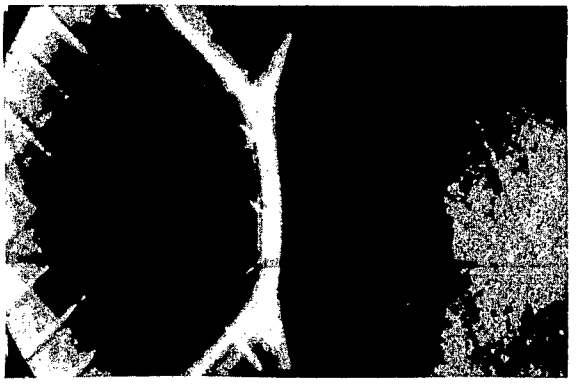

Figure 3c. In a Laval nozzle.

Figure 3. Branched shocks .

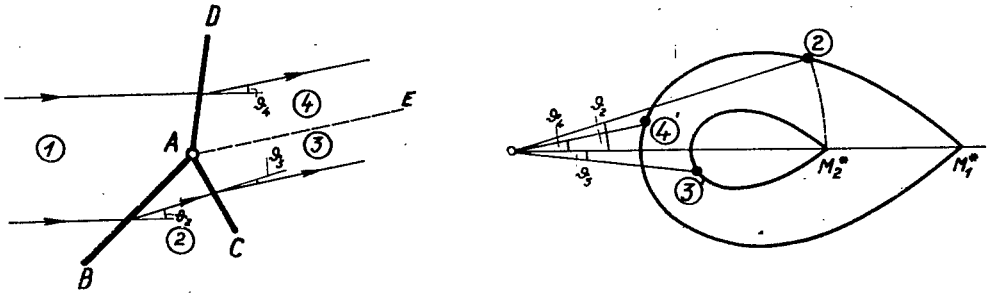

Figure 4. Flow field and shock-polar diagram.

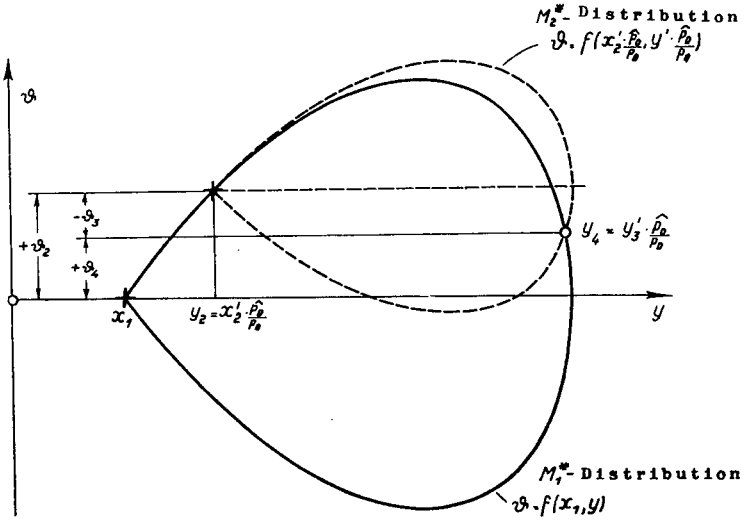

Figure 5. Construction of the solution.

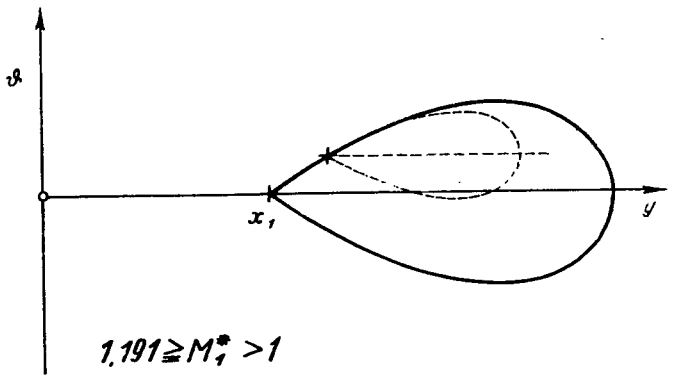

Figure 6.

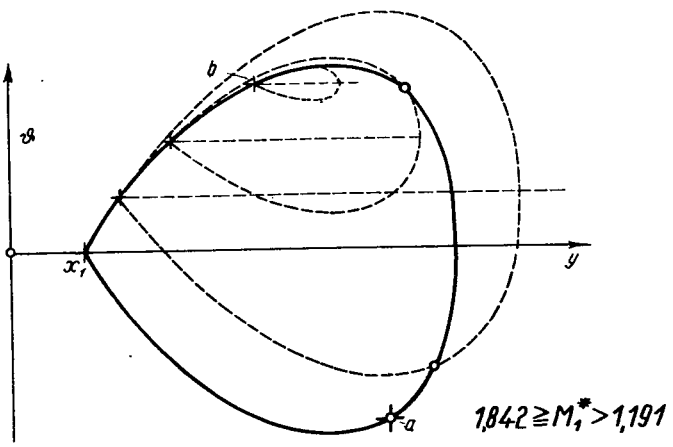

Figure 7.

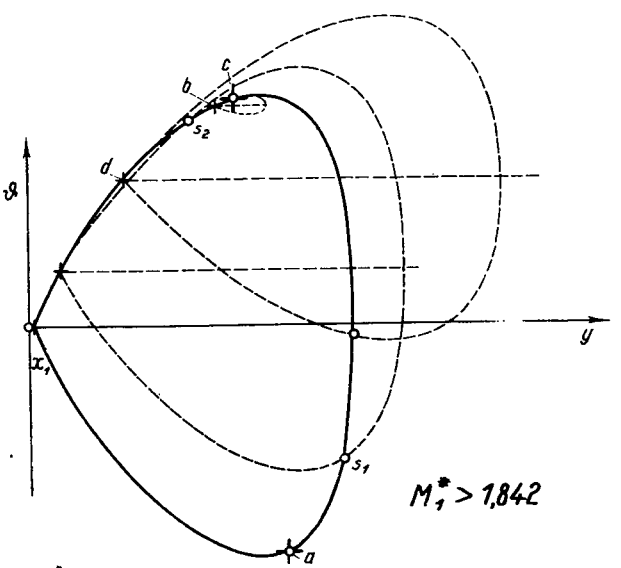

Figure 8.

Figures 6-8 The position of the intersection points in the intervals.

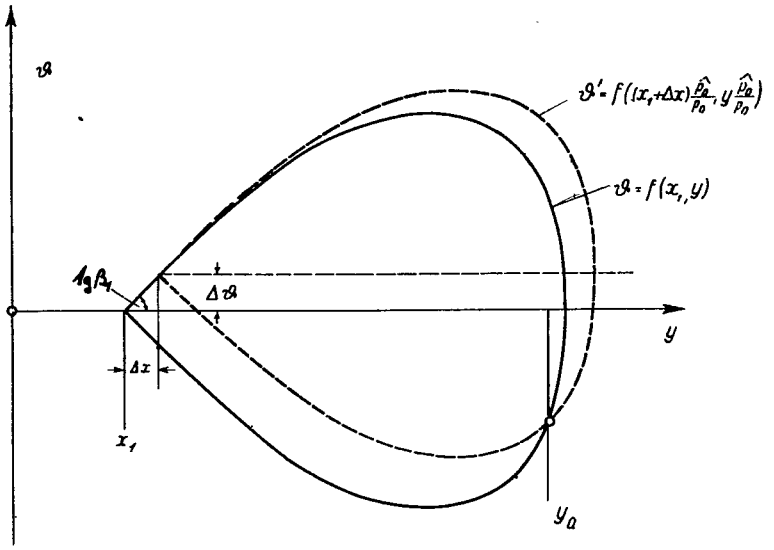

Figure 9. Determination of the limiting points a and c.

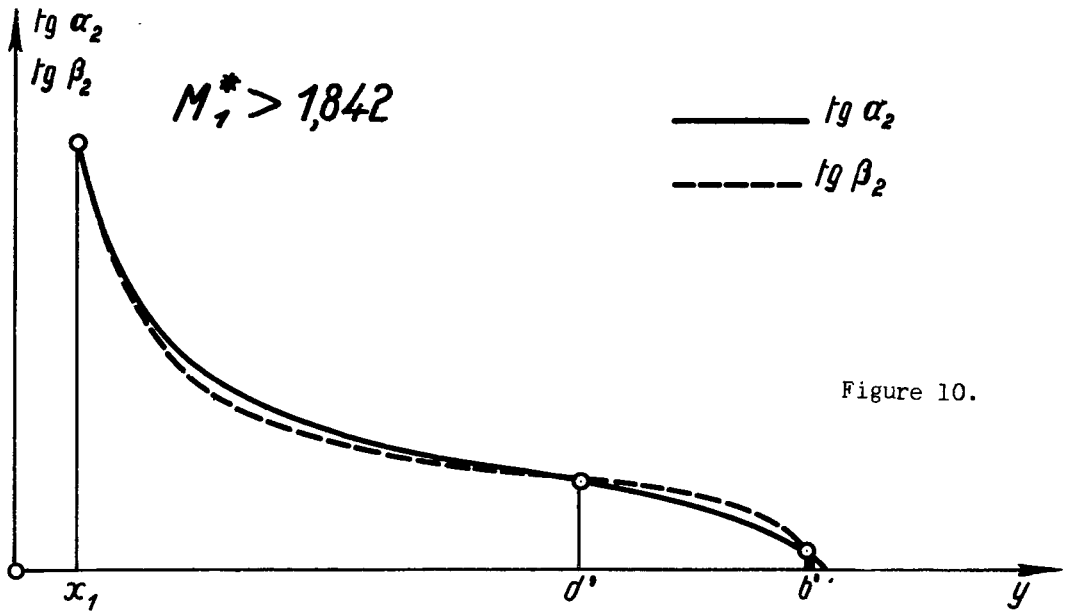

Figure 10.

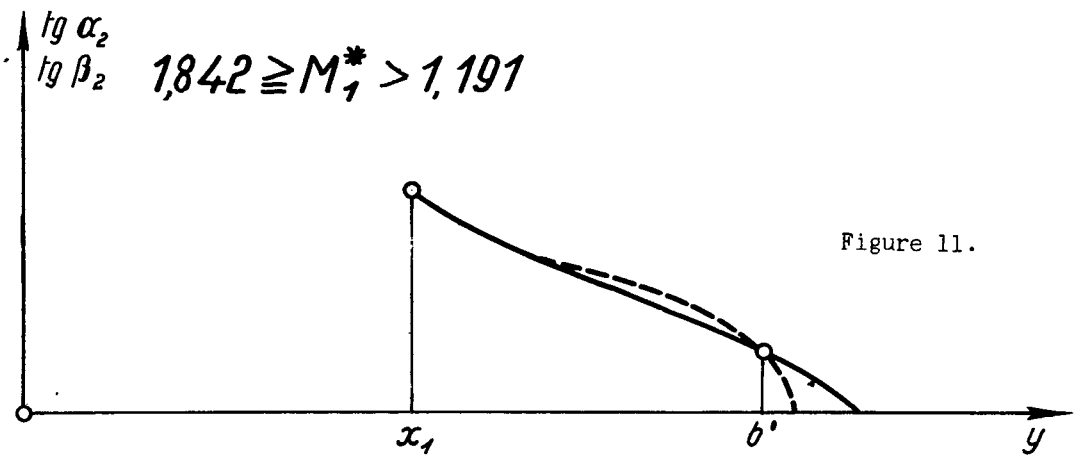

Figure 11.

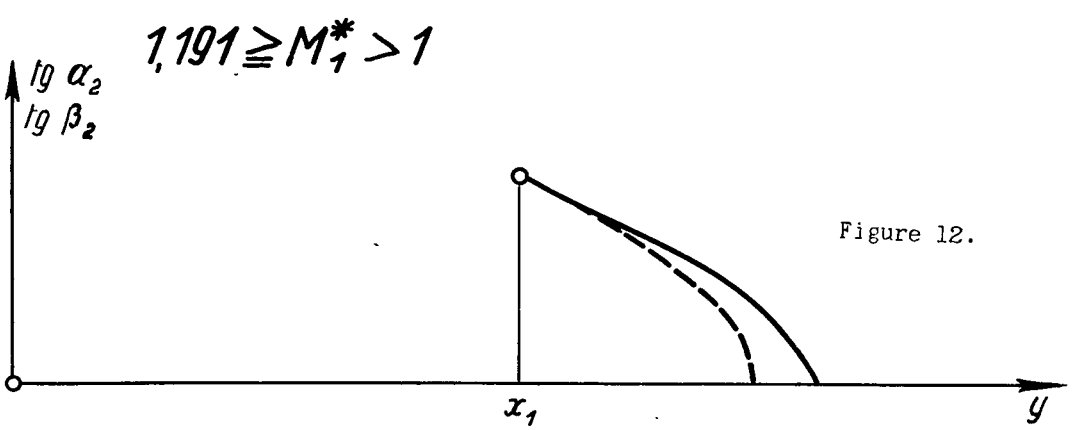

Figure 12.

Figures 10-12 Determination of interval limits.

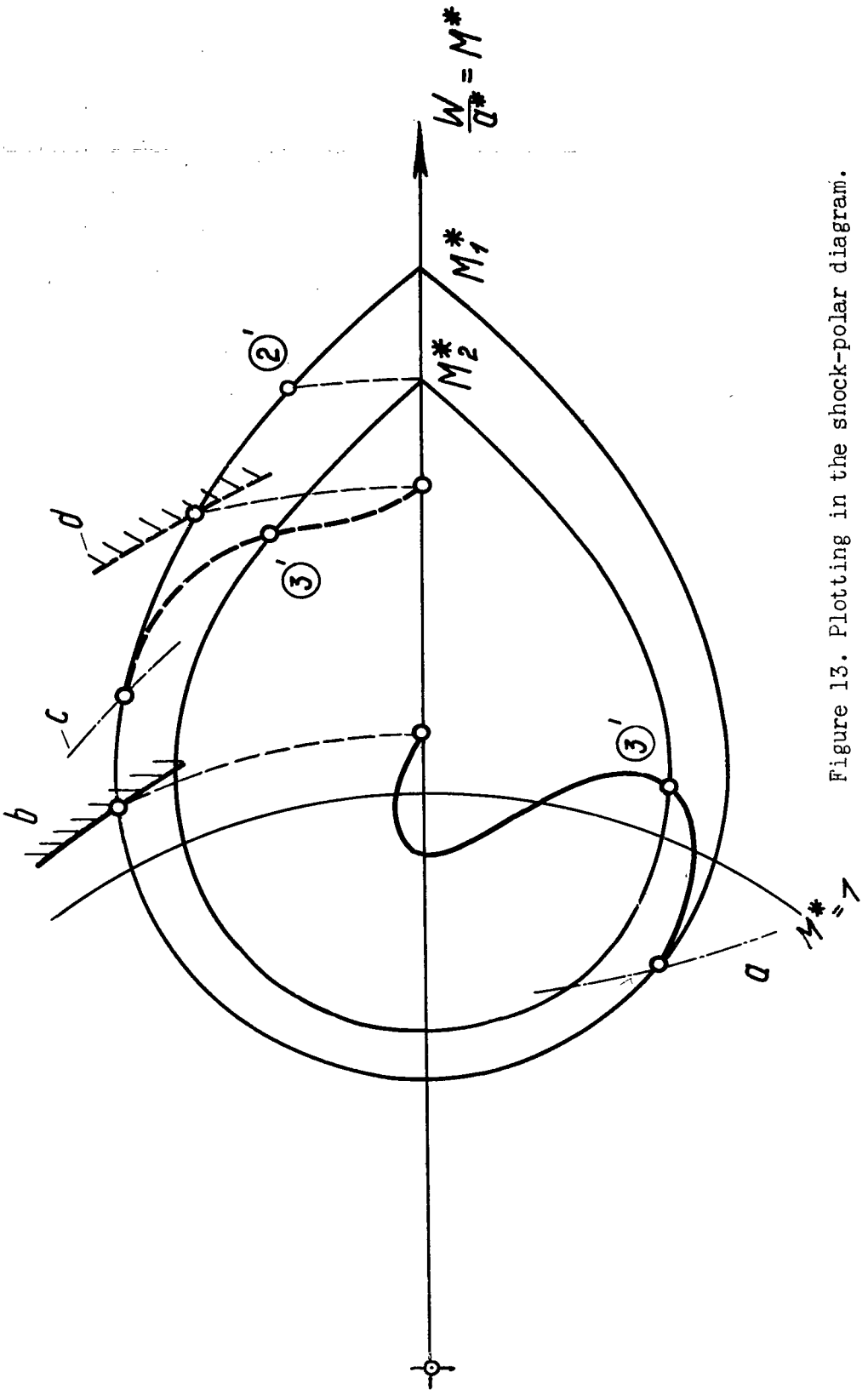

Figure 13. Plotting in the shock-polar diagram.

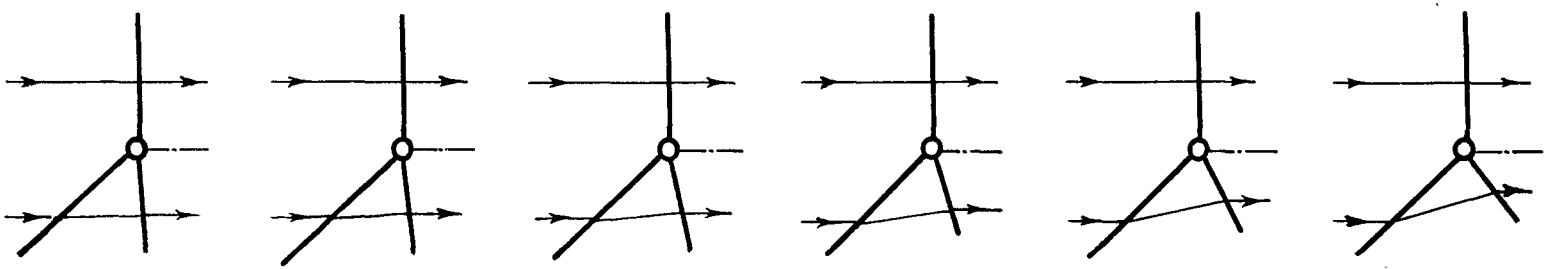

M_1^*	1,38	1,40	1,45	1,50	1,60	1,70
$\vartheta_2 = -\vartheta_3$	1,8°	2,7°	5,4°	7,5°	11,5°	14,8°
M_2^*	1,350	1,349	1,345	1,350	1,378	1,421
M_3^*	0,741	0,745	0,765	0,788	0,846	0,921
M_4^*	0,725	0,715	0,690	0,666	0,625	0,588

Figure 14. Branching with straight principal shock.

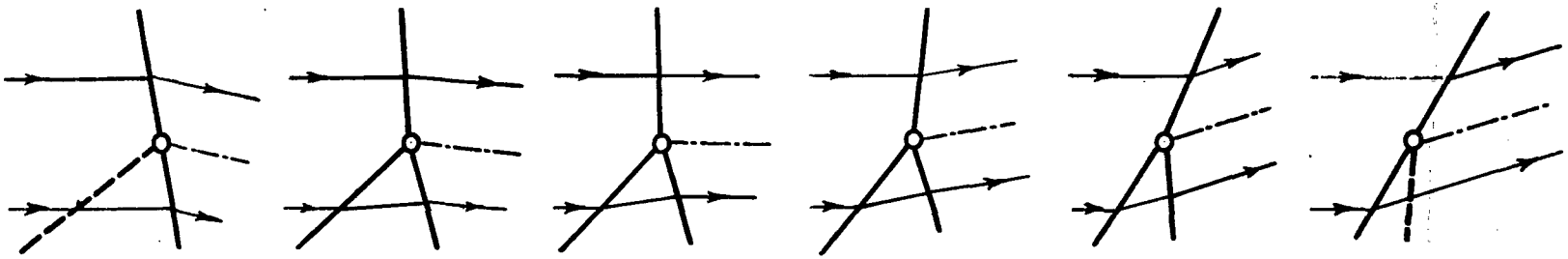

$M_1^* = 1{,}5$ $M_1 = 1{,}763$

ϑ_2	0	4°	8°	12°	15°	16,5°
M_2^*	1,50	1,421	1,335	1,231	1,126	1,062
ϑ_3	−11,4°	−10,0°	−6,9°	−2,8°	+2,3°	0,0°
M_3^*	0,720	0,759	0,792	0,823	0,920	1,062
ϑ_4	−11,4°	−6,0°	−1,1°	+9,2°	+17,3°	+16,5°
M_4^*	0,720	0,679	0,666	0,696	0,879	1,062

Figure 15. Example of a branching, with fixed flow.

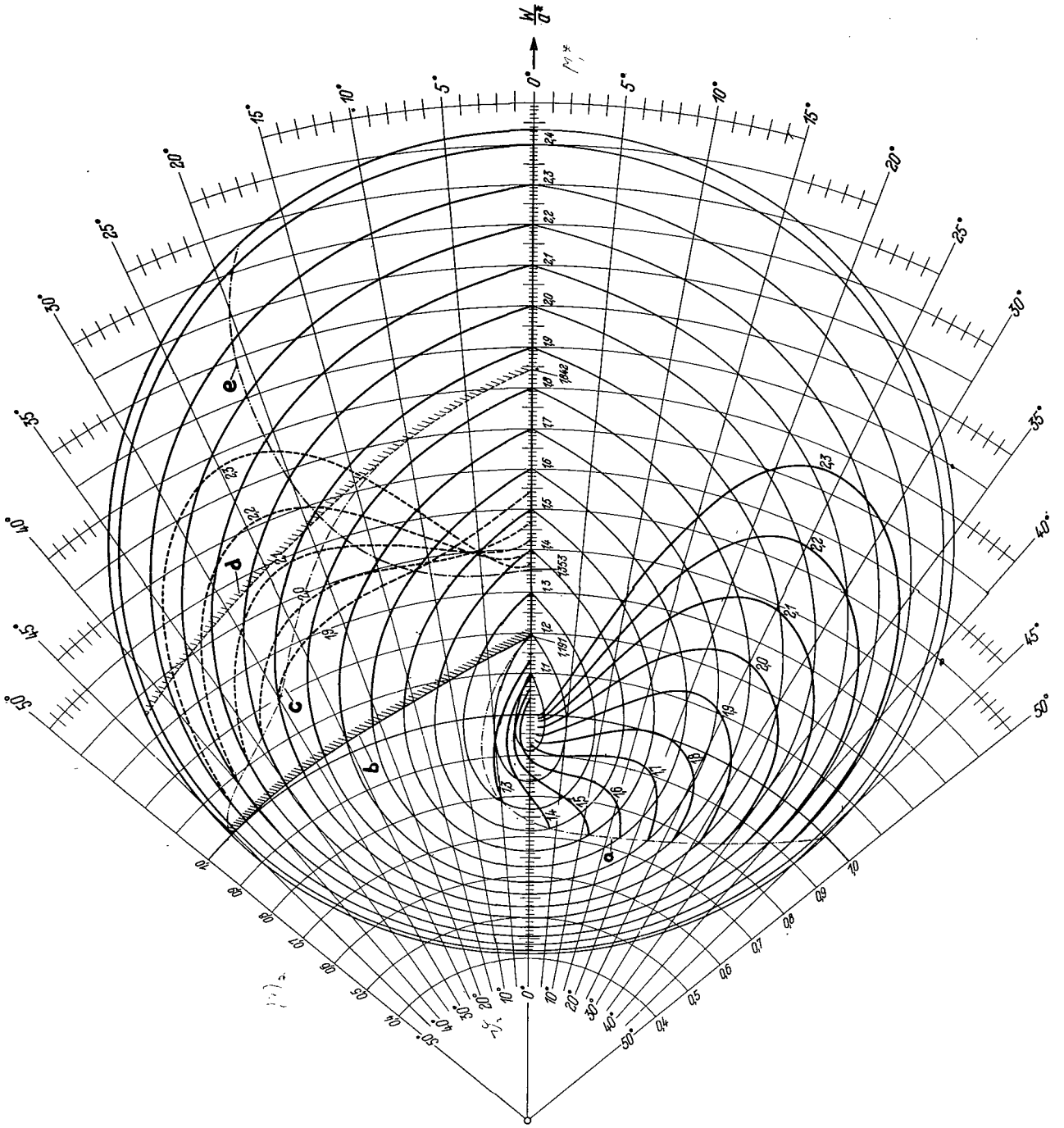

Appended chart: Polar-shock diagram for branched shocks.